

Chapter 2

Fatigue Analysis of 7075 Aluminum Alloy by Optoacoustic Method

Tomohiro Sasaki, Hiroshi Ono, Sanichiro Yoshida, and Shuich Sakamoto

Abstract The influence of fatigue damage on the elastic response of AA7075 aluminum alloy was investigated through a combination of optical and acoustical experiments. Specimens were previously subjected to fatigue cyclic loads at various fatigue levels within the fatigue life. Macroscopic deformation process under a certain load below the yield point (elastic region) for the pre-fatigued specimen was visualized by electronic speckle pattern interferometry (ESPI). At the same time, the acoustic velocities of vertical and shear waves propagating in the fatigued specimen were measured using an ultrasonic probe. The acoustic analysis showed the following change in residual stress by the fatigue cyclic load; an increase in compressive residual stress with the number of pre-fatigue cycles (N_P) below 10^3 , and relaxation of the residual stress N_P over 10^3 . The visualization using ESPI demonstrated that the strain heterogeneity in the macroscopic elastic regime was enhanced with increase of the pre-fatigue cycle. The correlation between the optical and the acoustical measurement results is discussed based on the change in the residual stress, localized plastic deformation, and the crack initiation.

Keywords Fatigue • Optical method • Acoustic method • Speckle pattern interferometry • Aluminum alloy

2.1 Introduction

Fatigue of metals is generally interpreted as a process of crack initiation by localized deformation, and crack propagation, leading to final fracture under cyclic loading. A number of fatigue inspection methods such as those use X-ray, ultrasonic wave, and acoustic emission have been established [1–4]. These methods mainly aim at detection of the presence of fatigue crack, and fatigue life is predicted by monitoring the crack length based on fracture mechanical parameters. On the other hand, the stage of localized plastic deformation prior to the crack initiation is a complex phenomenon and not fully understood. Thus, it is generally difficult to detect the fatigue damage at the earlier fatigue stage particularly in ductile metals, because most of the fatigue life is spent by the stage before the crack initiation. The localized plastic deformation occurs not only in “Low cycle fatigue”, but also in “High cycle fatigue” that is characterized by lower stress condition below the macroscopic yield stress. This study focuses on the influence of the localized plastic deformation on macroscopic deformation behavior of metals. Our previous works using a full field optical method [5, 6] demonstrated that the strain concentration, which is observed in the macroscopic elastic regime, is enhanced depending on the degree of fatigue cycles. On the other hand, a similar effect of fatigue damage on the elastic behavior of metals was also confirmed through acoustical methods by several researchers [7–10]. These methods are based on stress dependence of elastic wave velocity that propagates through the material, termed as “acousto-elasticity”. The fatigue damage was detected as a change in the elastic wave velocity or attenuation attributed to residual stress induced by the localized plastic deformation. Both the results obtained from the optical and the acoustical methods are associated with the elastic response of metals, and indicate the possibility of analyzing the elastic response as a mean of fatigue diagnosis.

T. Sasaki (✉) • H. Ono • S. Sakamoto
Graduate school of Niigata University, 8050 Ikarashi-nincho, Nishi-ku, Niigata-shi, Niigata, Japan
e-mail: tomox@eng.niigata-u.ac.jp

S. Yoshida
Department of Chemistry and Physics, Southeastern Louisiana University, SLU 10878, Hammond, LA, 70402, USA
e-mail: syoshida@selu.edu

In the present study, in order to establish the correlation of the elasticity of metals and the fatigue damage, the deformation behavior of aluminum alloys previously subjected to cyclic loading are visualized with electronic speckle pattern interferometry (ESPI). At the same time, the change of elasticity due to the fatigue damage is evaluated by the acoustic measurement. We demonstrate the influence of microscopic factors including the localized plastic deformation, the presence of micro-cracks, on strain heterogeneity, and discuss the change in elastic response of the material.

2.2 Experimental Procedure

2.2.1 Fatigue Test

An AA7075-T1 aluminum alloy sheet with thickness of 3.0 mm was used for experiments. Necked shape specimens as shown in Fig. 2.1 were cut from the sheet for fatigue tests by electronic discharge machining. The yield strength of specimen measured by a static tensile test was approximately 8.0 kN. The fatigue test was conducted for the specimen under load control condition with a sinusoidal waveform of 5 Hz. The maximum tensile load ranged from 5.0 kN to 7.0 kN, and the minimum load was a constant at 0.1kN. Figure 2.2 shows the maximum load – number of cycle curve obtained from the fatigue test. From this curve, the maximum load in the pre-fatigue test was determined to 5.0 kN which was approximately the fatigue limit. The numbers of cycles used in the pre-fatigue test, N_p , were 10, 10^2 , 10^3 , 10^4 , and 10^5 , respectively.

2.2.2 Acoustic Measurement

Acoustic wave velocity in the specimen was measured using an ultrasonic transducer driven by a square wave pulser-reciever with 35 MHz bandwidth (Olympus 5077PR). As shown in Fig. 2.3, the measurement was conducted for the necked center of specimen. Velocities of vertical wave propagating in the thickness direction (V_{zz}), and shear vertical waves in the displacement directions of x and y (V_{zx} , V_{zy}) were respectively measured. Coupling media used was distilled water for the vertical wave measurement, and glycerin paste for the shear wave measurement.

2.2.3 Dynamic Observation of Deformation Behavior of Pre-fatigued specimen

Deformation behavior during tensile tests was visualized with a two-dimensional ESPI in the same manner described in a previous work [6]. Figure 2.4 shows the optical setup in this study. Two optical interferometers were arranged to horizontal

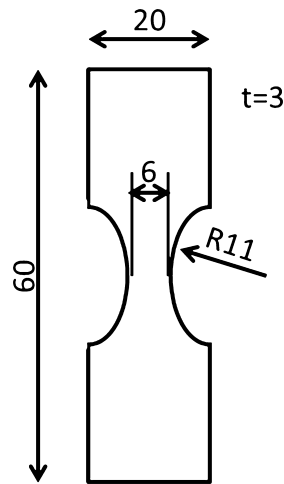


Fig. 2.1 Specimen used in this study

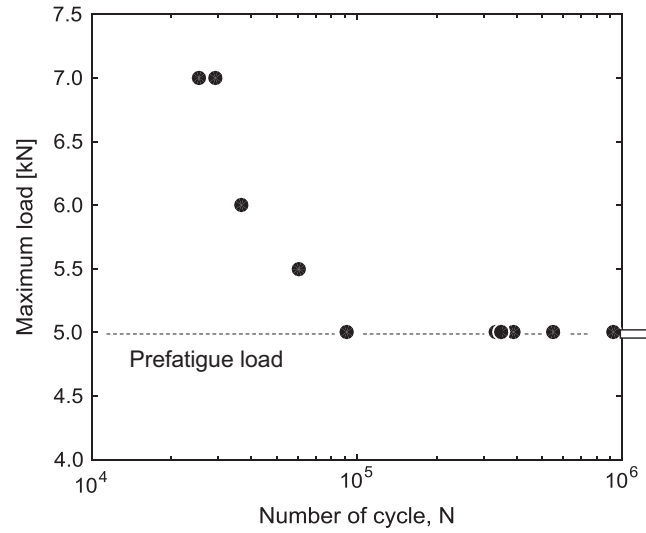


Fig. 2.2 Maximum load vs. number of cycle plot in the fatigue test

Fig. 2.3 Acoustic measurement

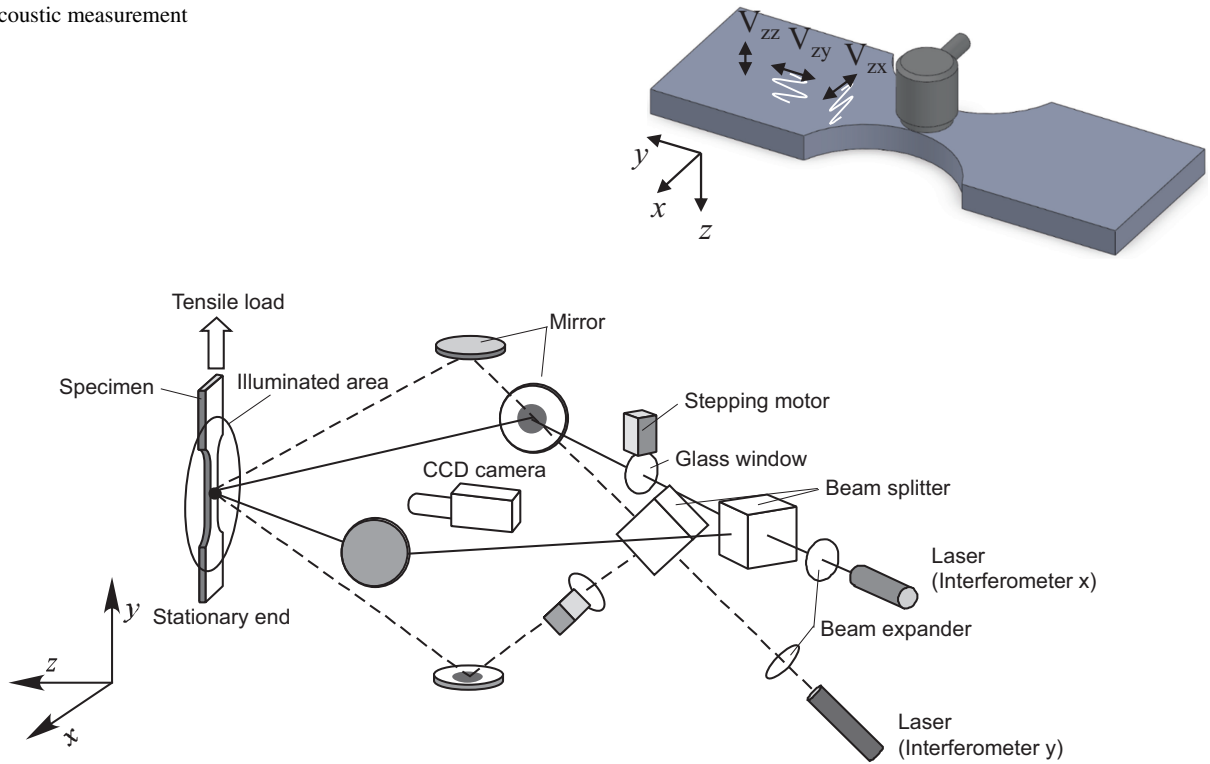


Fig. 2.4 Experimental arrangement of 2D-ESPI [6]

direction (x) and vertical direction (y) to the tensile machine (interferometer x , and interferometer y). Each interferometer was sensitive to in-plane displacement along its horizontal direction. Semiconductor laser with the wave length of 660 nm and the power of 50 mW was used for light source. The individual displacement fields in each sensitive direction were obtained by switching light sources of the two interferometers. The laser beam was expanded by a beam expander and split into two paths by a beam splitter and converged to the surface of specimen via two mirrors. The incident angles to the surface were 36.3° for the interferometer x , and 48.0° for the interferometer y . The speckle pattern was captured with a CCD camera with a frame rate of 15 frames per a second. The speckle intensity received by each pixel changes depending on the displacement in the sensitive direction due to optical path difference between the two interferometric arms. Thus, the displacement field on the measured surface can be obtained by computing the intensity difference as fringe contours.

In addition, a glass window with 5.2 mm thick and the refraction index of 1.53 was placed after the beam splitter for one interferometric arm of each interferometer, in order to introduce “a carrier fringe system” [11]. The optical distance of the laser beam which passes through the glass window varies depending on its incident angle. Since the beam is expanded by the expander, optical distance on the irradiated surface has a gradient. By rotating the window with a stepping motor, the carrier fringes orthogonal to the sensitive direction appear. The resultant fringe contours represents the superimposing displacement obtained from the carrier and the displacement, thus actual displacement can be obtained by subtracting the carrier from the measured fringe. The number of carrier fringes introduced to the measurement surface was 6 for the horizontal direction, x , and 3 for the tensile direction, y . Tensile load was applied up to 800 N (5% of the yield load), and the dynamic deformation behavior was measured.

2.3 Result and Discussion

2.3.1 Effect of Fatigue Cycle on Acoustic Wave Velocity

Figure 2.5 shows acoustic velocity plotted against logarithm of the number pre-fatigued cycles. The value of non-fatigued specimen ($N_P = 0$) is plotted to the pre-fatigue cycles, $N_P = 10^0$ for convenience. The vertical wave propagating in the thickness direction, V_{zz} , decreased as N_P increased up to 10^3 , then it increased again (Fig. 2.5a). In acousto-elastic theory, the elastic modulus depends on applied stress due to the non-linearity between the interatomic force and the interatomic distance [11]. In particular, tensile stress leads to a decrease in the sound velocity. Thus, the initial decrease in the V_{zz} at $N_P < 10^3$ is indicative of an increase of the tensile internal stress in the thickness direction, z . On the other hand, in the results of shear waves (Fig. 2.5b), although the change was relatively small, both V_{zx} and V_{zy} exhibited a slight increase at lower N_P , followed by a decrease in contrast to the change of V_{zz} . Toda et al. [12] proposed “R-value acoustoelastic method” that uses the ratio of vertical wave velocity and averaged value of shear wave velocity. According to this method, the ratio of V_{zz} and $(V_{zx} + V_{zy})/2$ is proportional to the sum of in-plane principle stress as shown below.

$$R = \frac{V_{zz}}{(V_{zx} + V_{zy})/2} = R_0 + C_R (\sigma_x + \sigma_y) \quad (2.1)$$

where R_0 is microstructural factor, C_R is stress-acoustic constant, σ_x , and σ_y are components of plane stress. Figure 2.6 shows the R value plotted against the pre-fatigue cycle. Since the R-value generally has a positive value, a decrease at

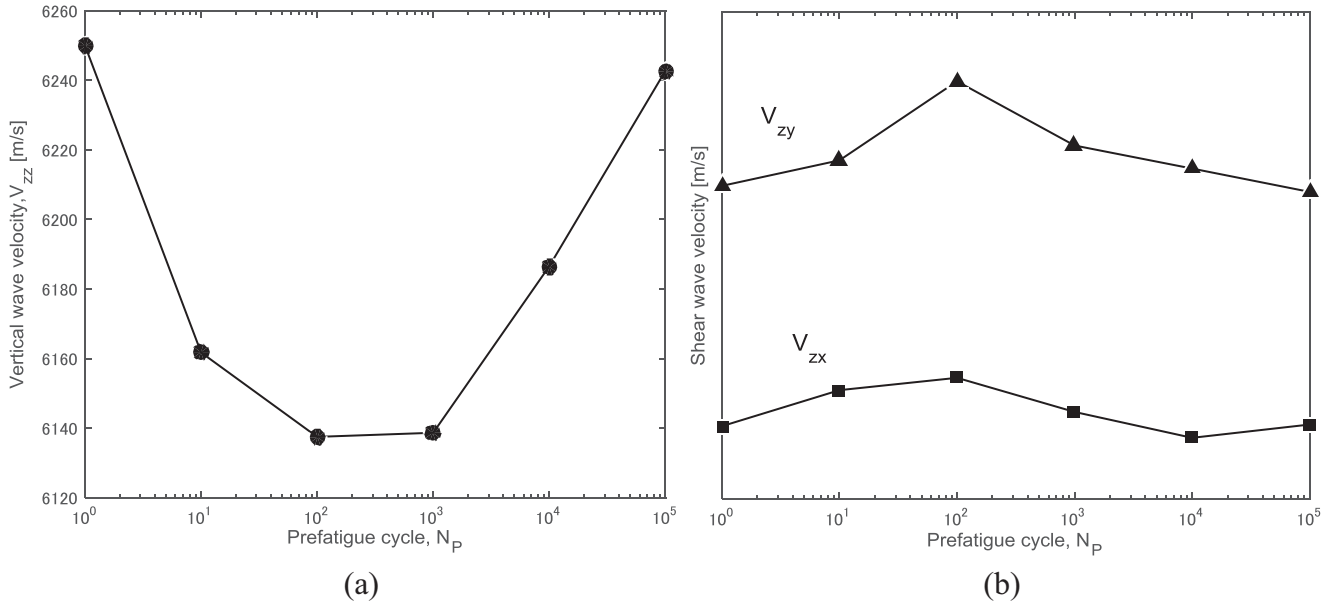


Fig. 2.5 Acoustic wave velocity for (a) vertical wave V_{zz} , and (b) shear vertical waves V_{zx} and V_{zy}

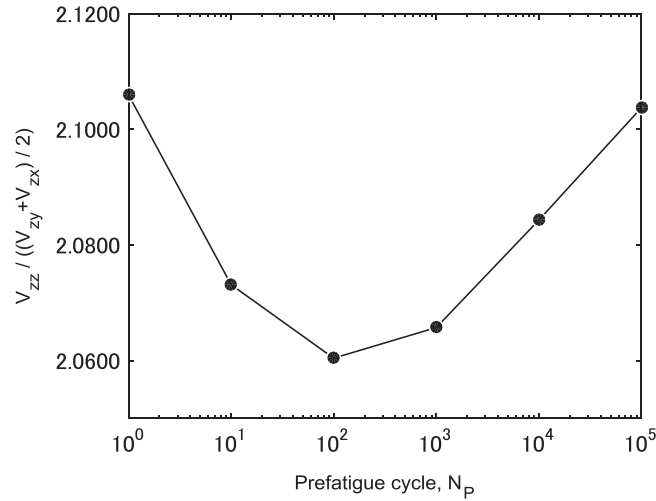


Fig. 2.6 The ratio of vertical and averaged shear wave velocity

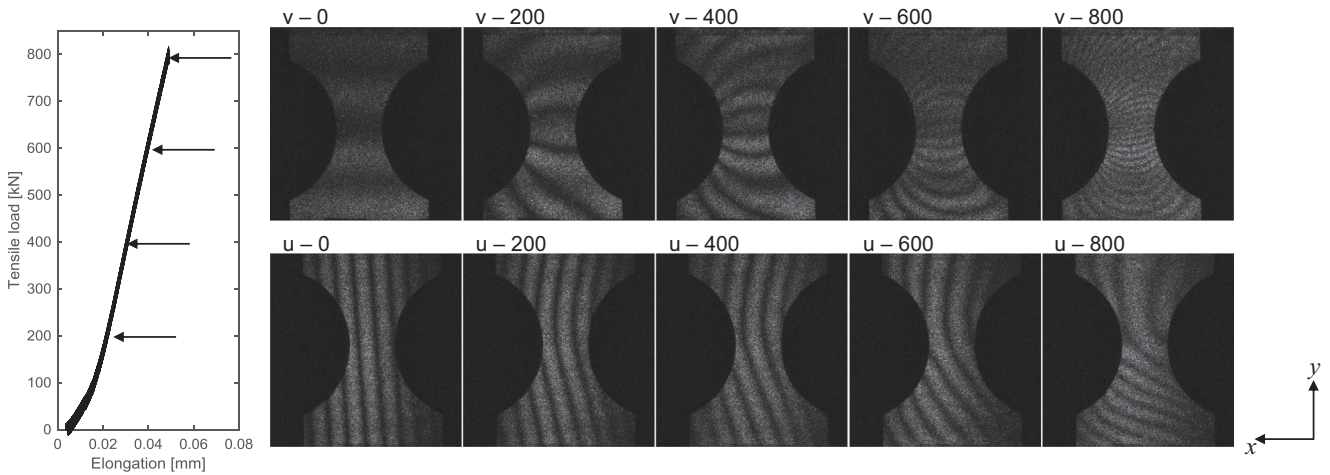


Fig. 2.7 Load-elongation curve and fringe pattern observed at various tensile loads of a non-fatigued specimen. The tensile load is indicated in the load – elongation curve by arrows

$N_p < 10^3$ implies an increase of compressive stress in the x-y plane. Cyclic tensile load during the pre-fatigue causes the localized plastic deformation in the necked area. This fact might result in the increase of compressive residual stress, because the deformed area is restrained by the surrounding area. Therefore, the earlier pre-fatigue stage of $N_p < 10^3$ can be interpreted as an increasing process of the residual stress in the necked part. Furthermore, the latter increase in the R-value at $N_p > 10^3$ indicates a relaxation of the residual stress. This relaxation behavior agrees with the result of surface acoustic wave velocity measurement by a scanning acoustic microscope in our previous work [6]. In the previous work, crack initiation was confirmed at the latter fatigue stage when the acoustic wave velocity decreased. It can be understood that the residual stress induced by the localized plastic deformation was relaxed with the crack initiation.

2.3.2 Deformation Behavior in Tensile Test

Figure 2.7 shows a load-elongation curve and optical fringe patterns observed in a tensile test of the non-fatigued specimen ($N_p = 0$). These fringe patterns represent displacement contours along x, and y resulting from subtracting captured images at various tensile load levels by a base image before the tensile test (tensile load = 0 N). Fringe pattern at 0 N (v-0 N or u-0 N) means the carrier fringes initially introduced. The fringe in the tensile direction y (v-fringe) concentrated to the neck

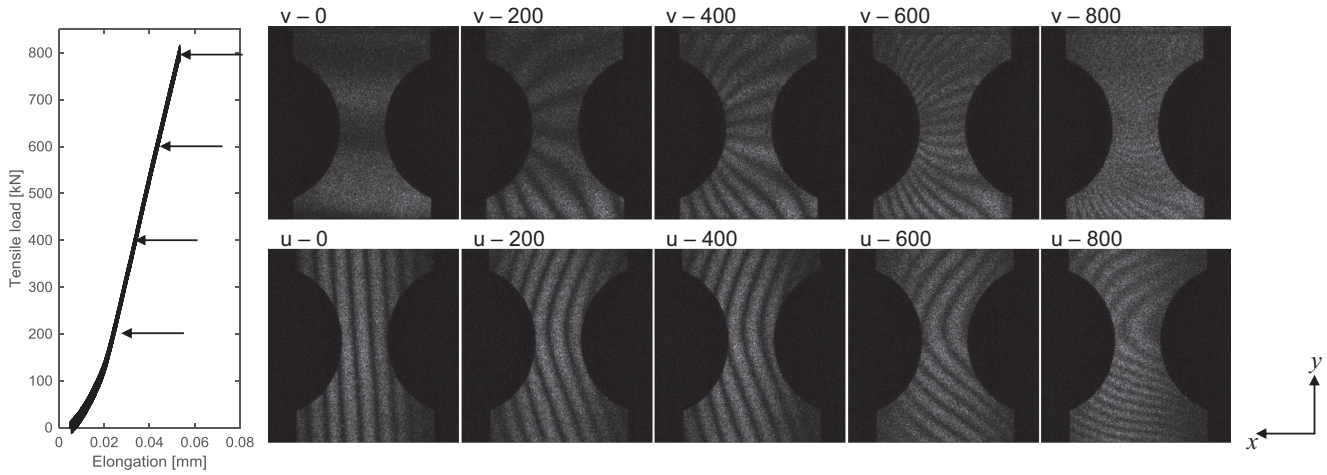


Fig. 2.8 Load-displacement curve and fringe pattern observed of a pre-fatigued specimen of $N_p = 10^5$

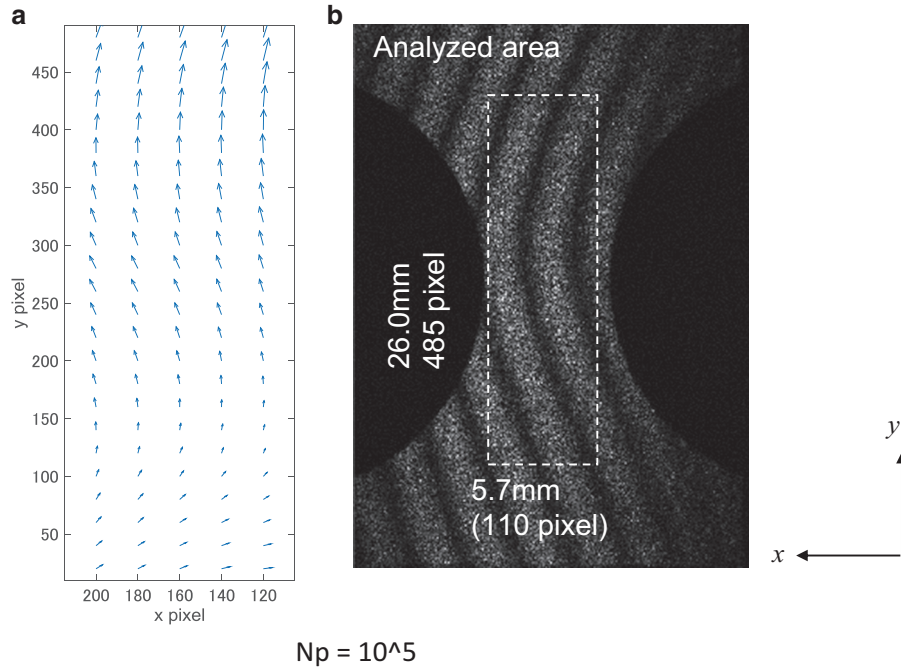


Fig. 2.9 Displacement vector field showing the deformation of necked part obtained from fringe analysis. The analyzed area is indicated in the image on the right

part of specimen with increase of tensile load, showing the strain concentration. In the horizontal direction, x (u -fringe), the initial carrier fringes gradually became a bent shape. Difference between the non-fatigue and pre-fatigued specimen was observed in this strain concentration behavior. Figure 2.8 shows an example of the fringe patterns in a tensile test for the pre-fatigued specimen ($N_p = 10^5$). In all the pre-fatigued condition, the pre-fatigued specimens basically exhibited a similar concentration behavior of the v -fringe, whereas the curvature of u -fringe tended to be higher than that in the non-fatigued specimen. Figure 2.9 shows displacement vector field of the necked part obtained from phase analysis of the u , and v fringe contours. The analysis was conducted for an area of 110×485 pixel ($5.7 \text{ mm} \times 26.0 \text{ mm}$) around the necked part indicated by dashed line. The quiver plot on the left indicates that the strain concentrates at one side of the neck, implying strain heterogeneity.

To discuss this strain concentration behavior in detail, the mean value of strain in the measured area was computed. Normal strain along the tensile axis ε_{yy} , and shear strain γ_{xy} were obtained from the displacement components v and u as follows.

$$\varepsilon_{yy} = \frac{\partial v}{\partial y}, \quad \gamma_{xy} = \frac{\partial u}{\partial y} + \frac{\partial v}{\partial x} \quad (2.2)$$

Figure 2.8 shows the result plotted against the tensile load up to 400 N. The tensile strain, ε_{yy} monotonically increased with the increases of applied load as shown in Fig. 2.9a. The pre-fatigued specimens exhibited higher slopes than that in the non-fatigued specimen. In addition, a larger difference was seen in the shear strain γ_{xy} as shown in Fig. 2.9b. The increase in γ_{xy} implies strain heterogeneity that is probably due to the localized plastic deformation during the fatigue test. The slopes of ε_{yy} and γ_{xy} , (compliance $d\varepsilon_{yy}/dF$ and $d\gamma_{xy}/dF$) obtained by a least square method are shown in Fig. 2.10. Variation of normal compliance, $d\varepsilon_{yy}/dF$ by the pre-fatigue cycle was consistent with the measurement result of shear velocity along the tensile direction (Fig. 2.5b); $d\varepsilon_{yy}/dF$ showed an increase at $N_p < 10^3$ and a decrease at $N_p > 10^3$. In addition, the shear compliance, $d\gamma_{xy}/dF$ showed a slight increase at $N_p > 10^3$ and a rapid increase at $N_p < 10^3$. These results demonstrate that the

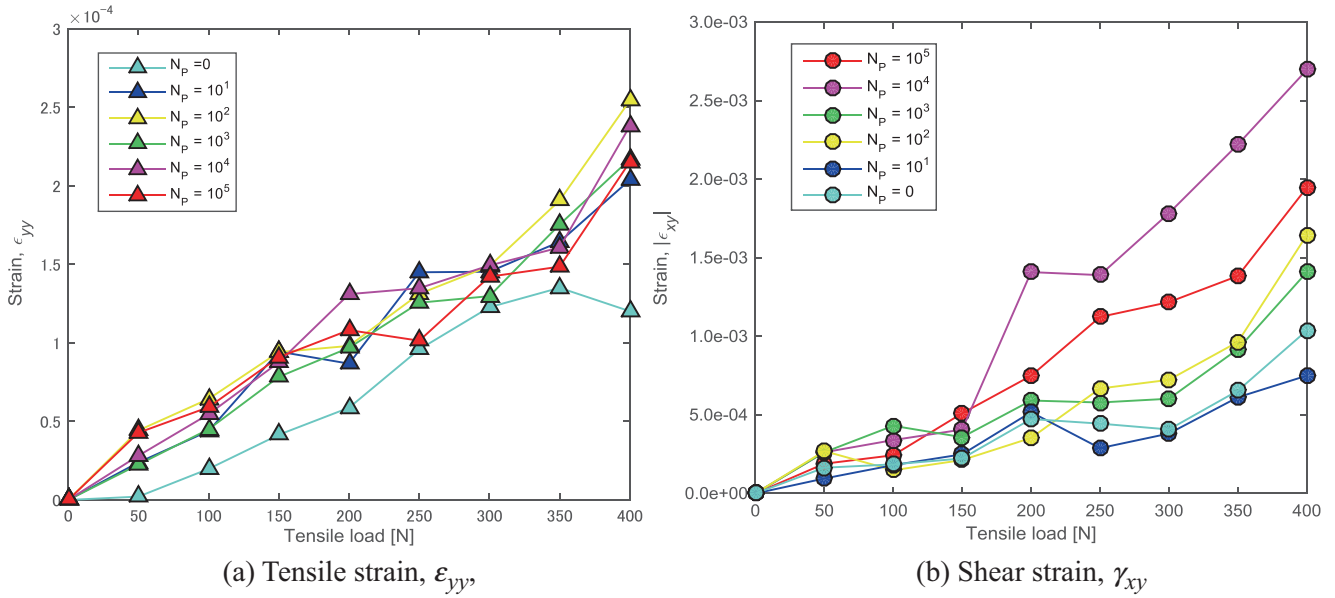


Fig. 2.10 Mean value of strain plotted against the applied load. (a) Tensile strain, ε_{yy} , (b) Shear strain, γ_{xy}

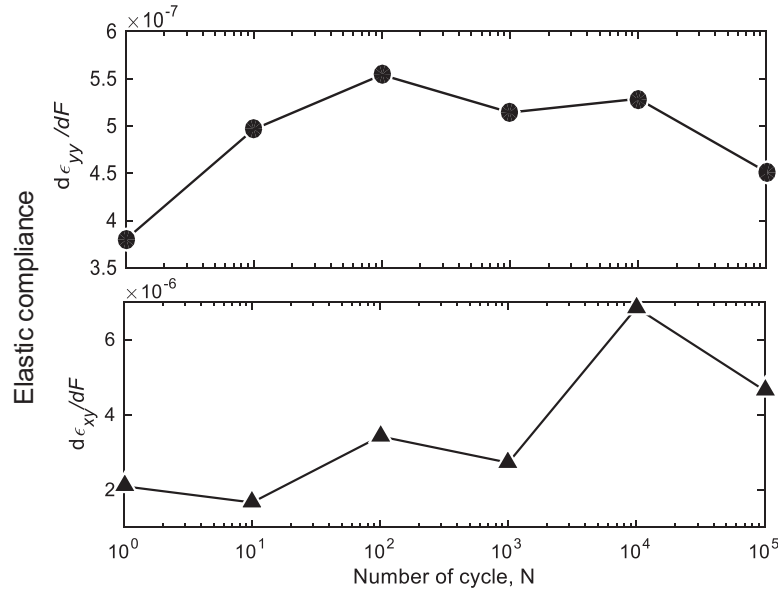


Fig. 2.11 Elastic compliance

fatigue damage due to the pre-fatigue load influenced elastic deformation behavior as well as the acoustic velocity. However, the acoustic measurement suggests the increase in the elasticity along the tensile direction by compressive residual stress (Fig. 2.6), and this is inconsistent with the increase in the elastic compliance $d\epsilon_{yy}/dF$. The discrepancy between the acoustic and the optical measurement can be explained by taking into consideration the effect of internal force by residual stress field described in another work [13]. The neck part of specimen is initially compressed by the surrounding region including both grip of specimen. When the specimen is stretched, the restoring force acts on the compressed region, resulting in decreasing the external tensile force. Consequently, the value $d\epsilon_{yy}/dF$ in the compressed region decreases. At the same time, the heterogeneity of residual stress in both side of the neck part of specimen may cause bending deformation. In the latter fatigue stage of $N_P > 10^3$, the residual stress is released by crack initiation, leading to the predominant shear deformation (Fig. 2.11).

2.4 Conclusion

The influence of fatigue damage on the elastic response of aluminum alloy has been investigated through acoustic wave velocity measurement and visualization of macroscopic deformation behavior using ESPI. In the earlier fatigue stage of pre-fatigue cycle $N_P < 10^3$, the change in the acoustic velocities suggested an increase of compressive residual stress along the tensile direction induced by the localized plastic deformation. On the other hand, the visualization of macroscopic deformation using ESPI demonstrated that strain heterogeneity in the macroscopic elastic regime was enhanced with increasing the pre-fatigue cycle, N_P . We infer that the residual stress induced by the fatigue cyclic load influenced the macroscopic deformation behavior. These results indicate that the fatigue damage at the earlier fatigue stage due to the localized plastic deformation can be detected by the macroscopic deformation behavior using ESPI.

References

1. Ogura, K., Miyoshi, Y., Kayama, M.: A study of X-ray analysis of fatigue fracture surface. *Eng. Fract. Mech.* **22**, 123 (1985)
2. Steuwer, A., Edwards, L., Pratihari, S., Ganguly, S., Peel, M., Fitzpatrick, M.E.: In situ analysis of cracks in structural materials using synchrotron X-ray tomography and diffraction. *Nucl. Instrum. Methods Phys. Res. B.* **246**, 246 (2006)
3. Steuwer, A., Rahman, M., Shterenlikht, A., Fitzpatrick, M.E., Edwards, L., Withers, P.J.: The evolution of crack-tip stresses during a fatigue overload event. *Acta Mater.* **58**, 4039 (2010)
4. Moorth, V., Jayakumar, T., Raj, B.: Influence of microstructure on acoustic emission behavior during stage 2 fatigue crack growth in solution annealed, thermally aged and weld specimens of AISI type 316 stainless steel. *Mater. Sci. Eng. A* **212**, 212 (1996)
5. Hasegawa, S., Sasaki, T., Yoahida, S., Hebert, S.L.: Analysis of fatigue of metals by electronic speckle pattern interferometry. *Conf. Proc. Soc. Exp. Mech.* **3**, 127 (2014)
6. Sasaki, T., Hasegawa, S., Yoahida, S.: Fatigue Damage Analysis of Aluminum Alloy by ESPI. *Conf. Proc. Soc. Exp. Mech.* **9**, 147 (2015)
7. Stratoudaki, T., Ellwood, R., Shrples, S., Clark, M., Somekh, M.G.: Measurement of material nonlinearity using surface acoustic wave parametric interaction and laser ultrasonics. *J. Acoust. Soc. Am.* **129**(4), 1721 (2011)
8. Rivière, J., Remillieux, M.C., Ohara, Y., Anderson, B.E., Haupt, S., Ulrich, T.J., Johnson, P.A.: Dynamic acousto-elasticity in a fatigue-cracked sample. *J. Nondestruct. Eval.* **33**, 216–225 (2014). doi:10.1007/s10921-014-0225-0
9. Su, Z., Zhou, C., Hong, M., Cheng, L., Wang, Q., Qing, X.: Acousto-ultrasonics-based fatigue damage characterization: linear versus nonlinear signal features. *Mech. Syst. Signal Process.* **42**, 25 (2014)
10. Eira, J.N., Vu, Q.A., Lott, M., Payá, J., Garnier, V., Payan, C.: Dynamic acousto-elastic test using continuous probe wave and transient vibration to investigate material nonlinearity. *Ultrasonics.* **69**, 29 (2016)
11. Yoshida, S., Sasaki, T., Craft, S., Usui, M., Haase, J., Becker, T., Park, I.-K.: Stress analysis on welded specimen with multiple methods. *Conf. Proc. Soc. Exp. Mech.* **3**, 143 (2015)
12. Toda, H., Fukuoka, H., Aoki, Y.: R-value acoustielastic analysis of residual stress in a seem plate. *Jpn. J. Appl. Phys.* **23**, 86 (1984)
13. Yoshida, S., Miura, F., Sasaki, T., Rouhi, S.: Optical analysis of residual stress with minimum invasion. In: Conference and Exposition on Experimental and Applied Mechanics, Indianapolis, USA, #141 (2017)

Tomohiro Sasaki Associate professor, The topics includes fatigue analysis, measurement of welding induced residual stress metals, using optical and acoustical techniques.

Advancement of Optical Methods in Experimental
Mechanics, Volume 3

Proceedings of the 2017 Annual Conference on
Experimental and Applied Mechanics

Lamberti, L.; Lin, M.-T.; Furlong, C.; Sciammarella, C.
(Eds.)

2018, VIII, 118 p. 109 illus., 82 illus. in color., Hardcover
ISBN: 978-3-319-63027-4